

Document downloaded from:

<http://hdl.handle.net/10251/144558>

This paper must be cited as:

Hernández-Montoto, A.; Llopis-Lorente, A.; Gorbe, M.; Terrés-Haro, JM.; Cao Milán, R.; Díaz De Greñu-Puertas, B.; Alfonso-Navarro, M.... (27-0). Janus Gold Nanostars- Mesoporous Silica Nanoparticles for NIR-Light-Triggered Drug Delivery. *Chemistry - A European Journal*. 25(36):8471-8478. <https://doi.org/10.1002/chem.201900750>



The final publication is available at

<https://doi.org/10.1002/chem.201900750>

Copyright John Wiley & Sons

#### Additional Information

"This is the peer reviewed version of the following article: Hernández Montoto, Andy, Antoni Llopis-Lorente, Mónica Gorbe, José M. Terrés, Roberto Cao Milán, Borja Díaz de Greñu, María Alfonso, et al. 2019. Janus Gold Nanostars Mesoporous Silica Nanoparticles for NIR-Light-Triggered Drug Delivery. *Chemistry - A European Journal* 25 (36). Wiley: 8471-78. doi:10.1002/chem.201900750, which has been published in final form at <https://doi.org/10.1002/chem.201900750>. This article may be used for non-commercial purposes in accordance with Wiley Terms and Conditions for Self-Archiving."

# Janus gold nanostars-mesoporous silica nanoparticles for NIR light-triggered drug delivery

Andy Hernández Montoto,<sup>[a]</sup> Antoni Llopis-Lorente,<sup>[a],[c]</sup> Mónica Gorbe,<sup>[a],[d]</sup> José M. Terrés,<sup>[a]</sup> Roberto Cao-Milán,<sup>[e]</sup> Borja Díaz de Greñu,<sup>[a],[c]</sup> María Alfonso,<sup>[a],[c]</sup> Javier Ibañez,<sup>[a]</sup> María D. Marcos,<sup>[a],[b],[c],[d]</sup> Mar Orzáez,<sup>[d]</sup> Reynaldo Villalonga,<sup>[f]</sup> Ramón Martínez-Máñez<sup>[a],[b],[c],[d]\*</sup> and Félix Sancenón<sup>[a],[b],[c],[d]</sup>

**Abstract:** Janus gold nanostars-mesoporous silica nanoparticles (AuNST-MSNs) nanodevices able to release an entrapped payload upon irradiation with near infrared (NIR) light are prepared and characterized. The AuNST surface is functionalized with a thiolated photolabile molecule (**5**), whereas the mesoporous silica face is loaded with a model drug (doxorubicin) and capped with proton-responsive benzimidazole-β-cyclodextrin supramolecular gatekeepers (**N1**). Upon irradiation with NIR-light, the photolabile compound **5** is photodissociated, resulting in the formation of succinic acid, which induces the opening of the gatekeeper and cargo delivery. In the overall mechanism, the gold surface acts as a photo-chemical transducer capable of transforming the NIR-light input into a chemical messenger (succinic acid) that opens the supramolecular nanovalve. The prepared hybrid nanoparticles are no cytotoxic to HeLa cells, until they are irradiated with a NIR laser, which lead to intracellular doxorubicin release and hyperthermia. This induced a remarkable reduction in HeLa cells viability.

The development of stimuli-responsive gated nanodevices based in the use of mesoporous silica has attracted remarkable attention due to their potential applications in several research fields such as payload controlled release,<sup>[1]</sup> new sensing/recognition protocols,<sup>[2]</sup> and abiotic communication processes.<sup>[3,4]</sup> These nanodevices are mainly composed by two subunits (i) an inorganic mesoporous silica support in which a cargo is entrapped and (ii) (supra)molecular entities grafted onto

the outer surface of the loaded solid.<sup>[5,6]</sup> The role of the (supra)molecular entities is to block the pores inhibiting cargo release until an external stimuli is applied. In this field, an increasing number of nanodevices have been designed in the last years for the selective delivery of selected cargos under physical (magnetic fields, ultrasounds, temperature, light, etc) or chemical (pH, enzymes, (bio)molecules, etc) stimuli allowing an on-command cargo release.<sup>[6]</sup>

One of the most studied applications of these gated systems is their use as nanodevices for controlled drug delivery.<sup>[7-12]</sup> Among different stimuli, nanodevices for controlled release in response to light irradiation are particularly appealing since cargo delivery can be triggered at-will by choosing the area and time of irradiation.<sup>[13,14]</sup> Moreover, the design of nanodevices able to release an entrapped drug using near infrared (NIR) light have remarkable interest due to the high penetration of NIR radiation and minimal damage to tissues.<sup>[15-17]</sup> Reported gated photo-triggered drug delivery systems based in these principles include the use of an inorganic porous solid (which is loaded with a selected payload) and an stimulus transducer which transforms light into a physical or chemical signal able to induce the controlled release of the cargo entrapped in the carrier. Maximizing the communication between these two structural elements is critical for enhancing the efficiency of the cargo release. Most of drug photo-triggered systems are designed to transform light into heat, where the latter is used as communication signal between components.<sup>[6]</sup> Such heat-based communication processes, however, are usually inefficient and demand high power irradiances for activating cargo release. As a result, the use of such drug photo-triggered systems may be limited in real biological applications. In this context, the development of different mechanisms of communication between both structural elements of drug photo-triggered systems may be appealing.

From another point of view, photolabile molecules (PLMs), which dissociate upon application of radiation, have been extensively used for the preparation of drug delivery nanodevices in recent years.<sup>[18-20]</sup> However, molecular photodissociation requires high energy radiations limiting their use in clinical applications.<sup>[21-25]</sup> In order to overcome these drawbacks, low energy radiations can be used for multi-photonic excitation of PLMs. This requires the use of high laser powers due to the low multiphoton absorbing cross sections of certain molecules.<sup>[26-29]</sup> As an alternative, electric field enhancement produced by localized surface plasmon resonance (LSPR) in metal nanoparticles has been reported to facilitate multiphoton excitation of PLMs even at low power irradiances.<sup>[30-32]</sup>

Taking into account the above mentioned facts, and as a proof of concept, we present here new nanodevices based on Janus-like nanoparticles<sup>[4,33-35]</sup> comprising of a gold nanostar (AuNST) as NIR light sensitizer,<sup>[36-39]</sup> and a gated mesoporous

[a] Dr. A. Hernández Montoto, Dr. A. Llopis-Lorente, M. Gorbe, J. M. Terrés, Dr. B. Diaz de Greñu, Dr. M. Alfonso, Dr. J. Ibáñez, Prof. M. D. Marcos, Prof. R. Martínez-Máñez, Dr. F. Sancenón  
Instituto Interuniversitario de Investigación de Reconocimiento Molecular y Desarrollo Tecnológico (IDM), Universitat Politècnica de València, Universitat de València (Spain). E-mail: rmaez@qim.es

[b] Dr. B. Diaz de Greñu, Dr. M. Alfonso, Prof. M. D. Marcos, Prof. R. Martínez-Máñez, Dr. F. Sancenón  
Departamento de Química, Universitat Politècnica de València, Camino de Vera s/n, 46022 Valencia (Spain).

[c] Dr. A. Llopis-Lorente, Dr. B. Diaz de Greñu, Dr. M. Alfonso, Prof. M. D. Marcos, Prof. R. Martínez-Máñez, Dr. F. Sancenón  
CIBER de Bioingeniería, Biomateriales y Nanomedicina (CIBER-BBN) (Spain).

[d] M. Gorbe, Prof. M. D. Marcos, Dr. M. Orzáez, Prof. R. Martínez-Máñez, Dr. F. Sancenón  
Unidad Mixta UPV-CIPIF de Investigación en Mecanismos de Enfermedades y Nanomedicina, Valencia, Universitat Politècnica de València, Centro de Investigación Príncipe Felipe, València, Spain.

[e] Dr. R. Cao-Milán  
Facultad de Química, Universidad de la Habana, 10400 La Habana (Cuba).

[f] Dr. R. Villalonga  
Department of Analytical Chemistry, Faculty of Chemistry, Complutense University of Madrid, 28040 Madrid (Spain).

silica nanoparticle (MSNP) as drug carrier. Drug delivery involves the use of multi-photon excitation of a 2-nitrobenzyl derivative grafted onto the AuNSt at low power irradiance and the generation of a “chemical messenger” which is able to communicate the AuNSt with the MSNP face, inducing payload delivery.

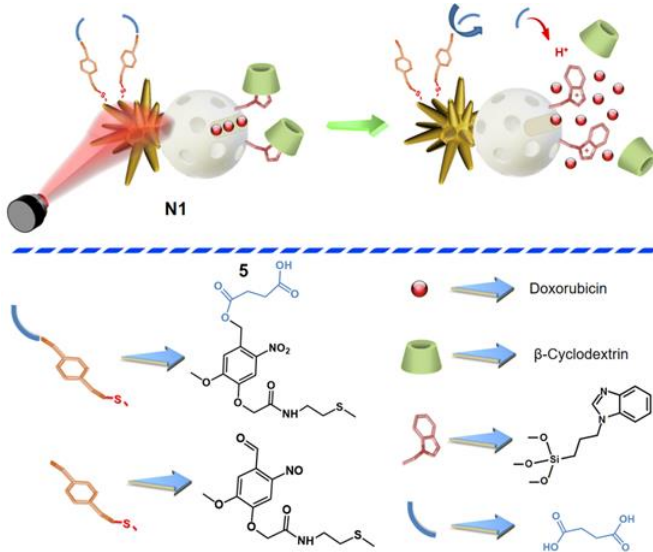


**Figure 1** Representation of nanodevice **N1** based on Janus AuNSt-MSNP and NIR light triggered drug delivery mechanism by photo-dissociation of 2-nitrobenzyl derivative **5**.

The design of the system is depicted in Figure 1. The nanodevice (**N1**) is functionalized with a thiolated 2-nitrobenzyl derivative (**5**) on the Au surface whereas the MSNPs are loaded with doxorubicin (Dox) and capped with an acid-sensitive benzimidazole-β-cyclodextrin gatekeeper.<sup>[40]</sup> Upon irradiation with an 808 nm laser, the AuNSt produce the multiphotonic excitation of the photolabile linker with the concomitant cleavage and release of succinic acid (chemical messenger). Subsequently, succinic acid induces the detreading of the supramolecular nanovalve, due to benzimidazole protonation, that result in cargo delivery from the MSNP. The gold surface acts as a photo-chemical transducer capable of transforming light into a chemical messenger (succinic acid) that triggers release from the mesoporous carrier. As far as we know, this new strategy for the light-induced delivery of drugs has not yet been reported, requires low power irradiances (*vide infra*) and can be used as an alternative to classical systems based in the transformation of light into heat.

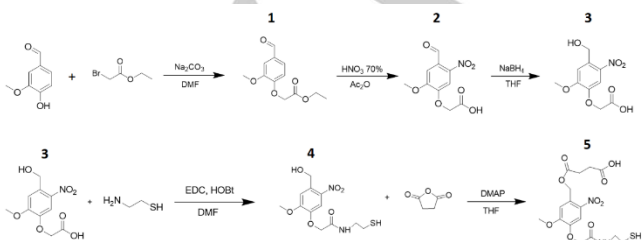


**Figure 2** Synthesis of photolabile molecule **5** bearing a 2-nitrobenzyl linker.

The thiolated photolabile molecule bearing a 2-nitrobenzyl linker coupled with succinic acid (**5**) was synthesized from vanillin in several steps (Figure 2). In a first step, alkylation of vanillin with ethyl bromoacetate quantitatively yields the

aldehyde-ester **1**. Then, nitration of compound **1**, carried out with nitric acid/acetic anhydride, yielded product **2**. Afterward, the aldehyde moiety in **2** was reduced using sodium borohydride yielding benzyl alcohol **3**. Subsequent amidation with cysteamine produced a 2-nitrobenzyl alcohol derivative bearing a thiol group **4**, which was coupled with succinic anhydride to produce the photolabile molecule **5**. The final and intermediate products were fully characterized by FT-IR and NMR spectroscopies (see Supporting Information). The thermal stability of **5** in solution (acetonitrile) was assessed by <sup>1</sup>H-NMR measurements. At this respect, no spectral changes were observed after heating **5** at 70 °C for 30 min.

AuNsts were obtained by a seeded growth method using polyvinylpyrrolidone (PVP) solution in *N,N*-dimethylformamide (DMF). This procedure is based on the chemical reduction of AuCl<sub>4</sub><sup>-</sup> complexes by DMF, and the subsequent deposition of gold atoms in the presence of PVP on the gold nanoparticles, acting as seeds.<sup>[36,37]</sup> Nanostars with size of 120 nm were synthesized using seeds (AuNPs) of 15 nm. Absorption spectrum of the obtained AuNsts showed a maximum in the NIR region at ca. 820 nm (Figure S1). AuNsts were dispersed in a solution of compound **5** in THF and finally were washed thoroughly to remove unbound molecules onto nanoparticle's surface. This yielded the intermediate nanoparticles **AuNSt@PLM-COOH** (Figure S2). The absorption of **AuNSt@PLM-COOH** slightly shifted to higher wavelength values due to the interaction of the gold surface with the thiol group of compound **5** (Figure S1).<sup>[37]</sup> Hydrodynamic diameter and zeta potential measurements by DLS, also confirmed the surface modification of AuNsts with **5**. The average hydrodynamic diameter of nanoparticles changed from 187 for AuNst to 158 nm for **AuNSt@PLM-COOH**, whereas the zeta potential changed from -27.6 to -30.5 mV (see Figure S3). The observed reduction in the average hydrodynamic diameter of AuNsts, upon functionalization with compound **5**, could be ascribed to the introduction of ionizable groups.

On the other hand, mesoporous silica nanoparticles (MSNPs) were prepared by alkaline hydrolysis and subsequent condensation of tetraethoxysilane (TEOS) using hexadecyltrimethylammonium bromide (CTAB) as a template (Figure S4).<sup>[41]</sup> Small angle powder X-ray diffraction (PXRD) patterns of MSNPs exhibited three peaks at  $2\theta = 2.50, 4.23$  and  $4.87^\circ$ , which could be indexed to (100), (110) and (200) diffraction planes of a hexagonal unit cell (Figure S5a). Moreover, N<sub>2</sub> adsorption-desorption isotherms of MSNPs showed a Type IV curve. From the curve a pore size of 2.5 nm was found, whereas the BET surface area and total pore volume were calculated to be 1088 m<sup>2</sup> g<sup>-1</sup> and 1.05 cm<sup>3</sup> g<sup>-1</sup>, respectively (Figure S5b).

Afterward, the MSNP's surface was partially masked by confining them at the interface of a water-wax emulsion and then functionalized with (3-mercaptopropyl) triethoxysilane (solid **HS-MSNP**).<sup>[33-35]</sup> The paraffin wax was dissolved in hexane and the external surface was further functionalized with (3-iodopropyl) trimethoxysilane (**HS-MSNP-I**) and then with benzimidazole (**HS-MSNP-Bzi**). Finally, the mesoporous phase was loaded with Dox and the pores were capped by the formation of a supramolecular complex between the grafted benzimidazole and β-cyclodextrin (**MSNP@Dox@Bzi-CD**).<sup>[34]</sup> Zeta potential values of the nanoparticles, measured by DLS, were used to monitor each reaction step (Figure S6). The zeta potentials decreased gradually during surface modification with (3-mercaptopropyl)triethoxysilane (**HS-MSNP**: -23.4 mV), (3-

iodopropyl)trimethoxysilane (**HS-MSNP-I**: -33.2 mV) and benzimidazole (**HS-MSNP-Bzi**: -37.8 mV). Moreover, the zeta potential increased from -37.8 to -13.8 mV after Dox loading and surface functionalization with  $\beta$ -cyclodextrin (**HS-MSNP@Dox@Bzi-CD**). In addition, an overall fraction of organic material in **HS-MSNP@Dox@Bzi-CD** nanoparticles was estimated to be 9.5 % by TGA (Figure S7).

Finally, **AuNSt@PLM-COOH** nanoparticles were attached to thiol groups on **MSNP@Dox@Bzi-CD** yielding the final nanodevice **N1**. TEM images (Figures 3a, b and S8) showed the mesoporous morphology of the MSNPs and the presence of the AuNsts in the Janus colloids. A detailed analysis of nanoparticle morphology and composition was carried out using high resolution transmission electron microscopy (HR-TEM) and dark field scanning transmission electron microscopy (DF-STEM) (Figures 3c, d, e and S8, S9, S10). A clear presence of Au, Si and C atoms was observed. Moreover, as shown in Figure 3f, the UV-visible spectrum of **N1** nanodevice presented a marked absorption band centered at ca. 810 nm. Small angle powder X-ray diffraction (PXRD) patterns of **N1** nanoparticles exhibited a clear peak at  $2\theta = 2.50^\circ$ , which could be indexed to (100) diffraction plane of a hexagonal unit cell (Figure 3g). In the wide-angle PXRD pattern, four Au diffraction peaks were clearly discerned at  $2\theta = 38.21, 44.48, 64.76$  and  $77.74^\circ$ , which can be assigned to (111), (200), (220), and (311) reflections of the face-centered cubic gold lattice, respectively. Furthermore, the average hydrodynamic diameter and the zeta potential of **N1** were found to be 188 nm and -27.5 mV, respectively (Figure S11), with good colloidal stability after 24 and 48 h (Figure S12). The fraction of organic matter in the Janus nanodevice **N1** was calculated to be 4.8 % by TGA (Figure S13).

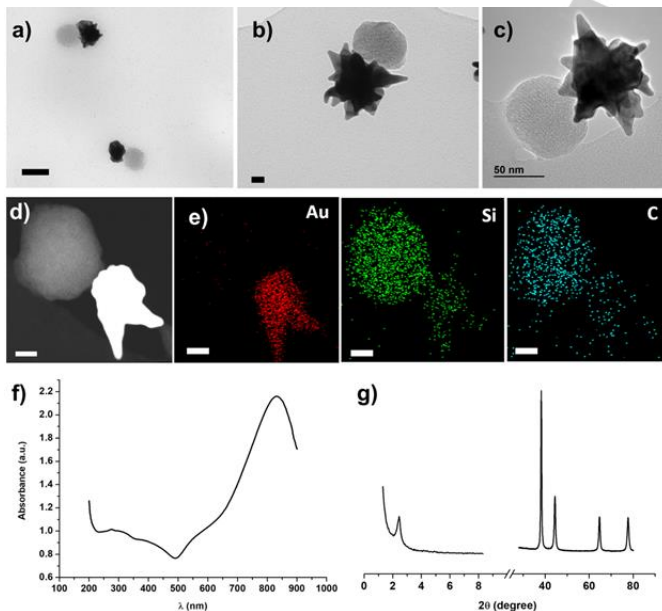


**Figure 3** (a,b) TEM, (c) HR-TEM and (d) STEM images of the Janus nanodevice **N1**. (d) EDXS element mapping analysis of Au, Si and C from STEM image. (Scale Bars: 100 nm (a), 20 nm (b,d,e)). (f) Optical extinction spectrum and (g) PXRD pattern of Janus nanoparticles **N1**.

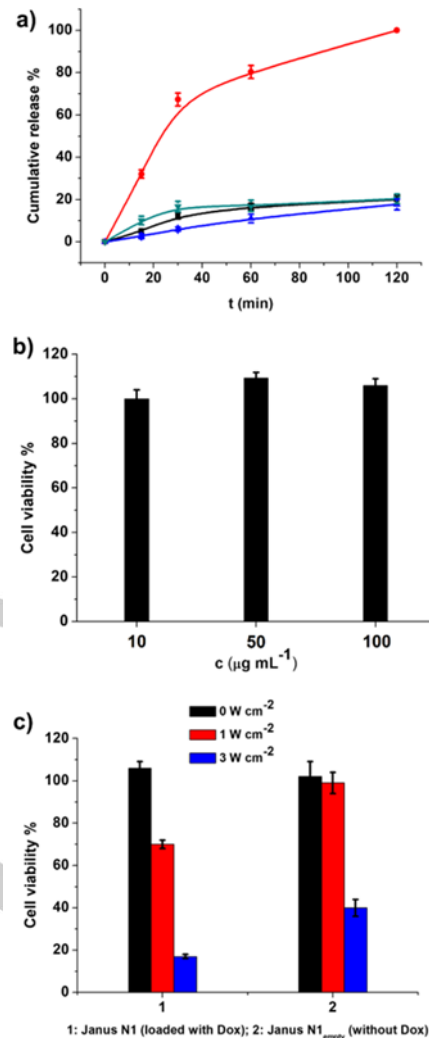


**Figure 4** (a) Cumulative release of Dox from **N1** in the presence (red) and absence (black) of NIR light, and from Dox-loaded Janus nanoparticles lacking compound **5** (in the AuNsts) in the presence (cyan) and absence (blue) of NIR light. (b) Cell viability of HeLa cells in the presence of Janus **N1** nanoparticles at different concentrations. (c) Cell viability of HeLa cells in the presence of Janus **N1** (loaded with Dox) and Janus **N1**<sub>empty</sub> (without Dox) nanoparticles at  $100 \mu\text{g mL}^{-1}$  upon 808 nm laser irradiation at different laser power densities for 10 min.

NIR light-triggered release experiments in aqueous suspensions of **N1** ( $0.1 \text{ mg mL}^{-1}$ ) were carried out by irradiation at 808 nm at low intensity ( $1 \text{ W cm}^{-2}$ ) whereas control samples were kept in the dark. At scheduled times, samples were centrifuged to remove the nanoparticles and the fluorescence spectra of released Dox at 555 nm was measured ( $\lambda_{\text{exc}} = 490 \text{ nm}$ ). As can be seen in Figure 4a, whereas in the absence of irradiation the release of Dox was negligible (black curve), a rapid and remarkable delivery was observed (ca. 80% of the total Dox delivered after 60 min) when nanoparticles were irradiated with NIR light (red curve). During the irradiation, compound **5** on AuNsts surface absorbs two low energy photons which activates a photo-redox reaction in the aromatic ring. This causes the reduction of nitro group and oxidation of the benzylic carbon, consequently producing C-O bond cleavage and succinic acid formation,<sup>[42]</sup> as confirmed by control experiments (Figures S14-S18). The “chemical messenger” succinic acid ( $pK_{a1} = 4.21$ ,  $pK_{a2} = 5.64$ ) induced protonation of

benzimidazole ( $pK_a = 5.55$ ) which produced dethreading of the benzimidazole- $\beta$ -CD inclusion complex and Dox delivery. Although previous studies have shown the desorption of ligands from gold surfaces induced by heat,<sup>[43]</sup> the temperature of **N1** suspensions upon NIR irradiation (Figure S19) remained relatively low (ca. 36 °C and 45 °C at 1 and 3 W cm<sup>-2</sup>, respectively) to be expected to produce derivative **5** direct desorption. To verify the proposed mechanism, we performed control release experiments with Janus **AuNST-MSNP** nanoparticles in which the AuNSTs were not functionalized with **5**. The obtained results are shown also in Figure 4a. As could be seen, Dox delivery was negligible both, in the absence of irradiation (blue curve) or upon irradiation (cyan curve). This pointed out the key role played by derivative **5**.

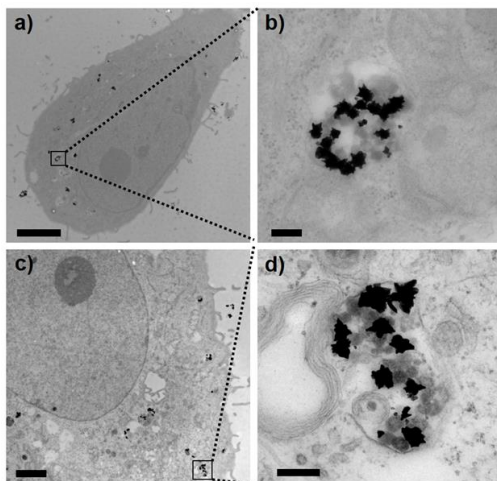


**Figure 5** TEM images of HeLa cells after incubation with Janus **N1** nanoparticles. Scale bars: (a) 5  $\mu$ m, (c) 2  $\mu$ m, (b,d) 200 nm.

As a further step, we evaluated the potential application of Janus **N1** nanoparticles for light-induce delivery of Dox in cancer cells. First, the internalization of **N1** nanoparticles in HeLa cells was tested using TEM. An efficient nanoparticle uptake by cells was produced after their incubation with a **N1** suspension in DMEM supplemented with 10% FBS. As can be seen in Figure 5, Janus **N1** nanoparticles were found inside cell endosomes. Next, cell viability of **N1** was determined using a WST-1 assay after incubation with nanoparticles at different concentrations (10, 50 and 100  $\mu$ g mL<sup>-1</sup>) for 48 h. The obtained results are shown in Figure 4b. Janus **N1** nanoparticles show almost no cytotoxicity toward HeLa cells in the three concentrations tested, thus demonstrating that Dox was efficiently encapsulated inside the mesoporous silica phase in **N1**. Once assessed the non-toxicity and the efficient uptake of **N1** nanoparticles we carried out NIR light triggered *in vitro* Dox release studies in HeLa cells. In a typical experiment, HeLa cells were incubated with **N1** or with Janus nanoparticles without payload (**N1<sub>empty</sub>**) and then irradiated with a laser at different power densities. After irradiation, cells were further incubated for 48 h and cell viability was then evaluated. As could be seen in Figure 4c, the viability of HeLa cells treated with **N1** and irradiated with NIR light at low power density (1 W cm<sup>-2</sup>) decreased (ca. 30%), whereas viability of cells incubated with **N1<sub>empty</sub>** remained near 100% after laser irradiation at 1 W cm<sup>-2</sup>. This suggests that decrease in cell viability in the presence of **N1** upon irradiation at low power density is mainly due to Dox release and not to hyperthermia. In contrast, viability of cells treated with **N1** or **N1<sub>empty</sub>** and

irradiated at high power density (3 W cm<sup>-2</sup>) decreased significantly in both cases, although a larger decrease in cell viability was observed for **N1** most likely due to a combined effect of hyperthermia (Figure S19) and Dox delivery.

Finally, NIR light triggered release of Dox from Janus **N1** nanocarriers in HeLa cells was tested using confocal laser scanning microscopy. Cells were stained with the DNA-marker dye Hoechst 33342 and the intracellular delivery of Dox after laser irradiation (power density of 1 W cm<sup>-2</sup>) was monitored (Figure 6a). A negligible Dox fluorescence signal was observed in non-irradiated samples. However, a marked 15-fold increase of Dox fluorescence in cells was evidenced after laser irradiation, corroborating the intracellular cargo release from **N1** triggered by NIR light (Figure 5b). Besides, the intracellular release of Dox from Janus **N1** nanoparticles was also triggered by *in situ* irradiation at 633 nm using the confocal laser scanning microscope (Figure S20). These results demonstrated the Dox release in cells induced by NIR irradiation and attributed to a multiphotonic excitation of compound **5** onto AuNSTs surface. Janus **N1** nanoparticles are a suitable platform for combined NIR light triggered drug delivery and hyperthermia in cancer therapy applications.

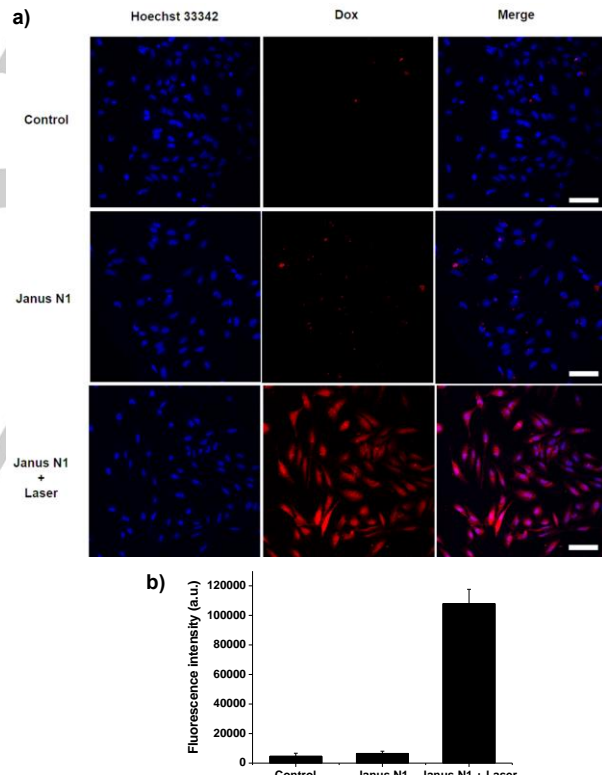


**Figure 6** (a) NIR light triggered release of Dox from Janus **N1** nanoparticles in HeLa cells monitored by confocal laser scanning microscopy. From left to right: DNA marker (Hoechst 33342), Dox, and combined (merge) fluorescence channels. From top to down: control cells (control), non-irradiated cells after incubation with nanoparticles (Janus **N1**) and NIR light irradiated cells after incubation with nanoparticles (Janus **N1** + Laser). Scale bars: 100  $\mu$ m. (b) Quantification of the Dox intensity delivered from Janus **N1** nanoparticles by confocal images analysis.

In conclusion, we reported herein the design, synthesis and characterization of a NIR-light responsive delivery system. The nanodevice consists of Janus-like nanoparticles with gold nanostars and mesoporous silica on opposite sides (**AuNST-**

**MSNP**). The gold surface is functionalized with **5**, a 2-nitrobenzyl derivative, whereas the MSNP is loaded with Dox and capped with a proton-responsive supramolecular nanovalve. Upon application of NIR light, 2-nitrobenzyl derivative molecules on the gold surface are dissociated giving succinic acid (chemical messenger) that induces the opening of the nanovalve and cargo delivery from the mesoporous face. The hybrid nanoparticles show no cytotoxicity toward HeLa cells. NIR irradiation at low power density ( $1 \text{ W cm}^{-2}$ ) resulted in Dox delivery and a reduction in cell viability. Moreover, irradiation at higher power density ( $3 \text{ W cm}^{-2}$ ) induced a larger cell viability decrease most likely due to a combined effect of hyperthermia and Dox delivery. We hope that this novel strategy for drug photodelivery could open new directions toward the development of NIR-induced delivery of cytotoxics. Inspired by these results, a variety of NIR light-triggered delivery systems can be obtained based on Janus **AuNSt-MSNP** by combining other gated ensembles on the MSNP and PLMs as transducer molecules on the gold surface.

## Experimental Section

**Synthesis of compound 1.** A mixture of vanillin (2.5 g, 16 mmol), ethyl bromoacetate (2 mL, 3 g, 18 mmol) and sodium carbonate (3.5 g, 25 mmol) in DMF (15 mL) was stirred at room temperature for 24 h. Water was added, and the mixture was partitioned between ethyl acetate and saturated NaCl solution. The organic phase was dried with anhydrous  $\text{Na}_2\text{SO}_4$  and evaporated to yield the aldehyde-ester **1** (3.5 g, 15 mmol, 90 % yield) as a white solid (Scheme S1).  $^1\text{H-NMR}$  (400 MHz,  $\text{CDCl}_3$ )  $\delta$  9.83 (s, 1H), 7.41 (d,  $J=1.9$ , 1H), 7.39 (dd,  $J=8.1$ , 1.9, 1H), 6.86 (d,  $J=8.1$ , 1H), 4.75 (s, 2H), 4.24 (q,  $J=7.1$ , 2H), 3.92 (s, 3H), 1.26 (t,  $J=7.1$ , 3H);  $^{13}\text{C-NMR}$  (100 MHz,  $\text{CDCl}_3$ )  $\delta$  190.9, 168.1, 152.6, 150.1, 131.2, 126.2, 112.5, 110.0, 66.0, 61.7, 56.1, 14.2.

**Synthesis of compound 2.** A solution of aldehyde-ester **1** (3.5 g, 15 mmol) in acetic anhydride (10 mL) was added to a cooled solution of 70 %  $\text{HNO}_3$  (10 mL) and acetic anhydride (15 mL) at 0 °C. The resultant mixture was stirred for 2 h and then allowed to warm to room temperature and stirring was continued for an additional 4 h. The reaction mixture was poured into a cold water, the pH adjusted with solid NaOH to 13–14 and then with 36 % HCl to 2–3. The aqueous phase was extracted with EtOAc and the organic phase dried and evaporated to yield a yellow solid. Recrystallization from  $\text{MeOH}/\text{H}_2\text{O}$  afforded the product nitro-acid **2** (3 g, 12 mmol, 80 % yield) (Scheme S1).  $^1\text{H-NMR}$  (400 MHz,  $\text{CDCl}_3$ )  $\delta$  10.24 (s, 1H), 7.40 (s, 1H), 7.24 (s, 1H), 4.66 (s, 2H), 3.86 (s, 3H);  $^{13}\text{C-NMR}$  (100 MHz,  $\text{CDCl}_3$ )  $\delta$  187.4, 168.9, 153.3, 150.4, 143.1, 126.0, 110.1, 108.7, 65.6, 56.5.

**Synthesis of compound 3.** To a solution of nitro-acid **2** (1 g, 4 mmol) in THF (20 mL)  $\text{NaBH}_4$  (0.5 g, 13 mmol) was added at room temperature. The reaction mixture was stirred for 24 h. Water was added and the pH adjusted with HCl (1M) to 2–3. The aqueous phase was extracted with EtOAc and the organic phase dried and evaporated to yield a pale yellow solid **3** (0.95 g, 3.7 mmol, 95 % yield) (Scheme S1).  $^1\text{H-NMR}$  (400 MHz,  $\text{CO}(\text{CD}_3)_2$ )  $\delta$  7.73 (s, 1H), 7.54 (s, 1H), 4.99 (s, 2H), 4.87 (s, 2H), 4.00 (s, 3H);  $^{13}\text{C-NMR}$  (100 MHz,  $\text{CO}(\text{CD}_3)_2$ )  $\delta$  169.8, 155.4, 146.8, 139.7, 136.0, 111.5, 111.2, 66.5, 61.8, 56.7.

**Synthesis of compound 4.** A mixture of solid **3** (0.25 g, 1 mmol), cysteamine (0.083 g, 1.1 mmol), HOEt (0.145 g, 1.1 mmol), EDC (0.21 g, 1.1 mmol) and triethylamine (0.15 mL, 0.11 g, 1.1 mmol) in DMF (5 mL) was stirred for 24 h at room temperature. The reaction mixture was partitioned between ethyl acetate and saturated NaCl solution. The organic phase was dried and evaporated to yield solid **4** (0.24 g, 0.75 mmol, 75 % yield) (Scheme S1).  $^1\text{H-NMR}$  (400 MHz,  $\text{CO}(\text{CD}_3)_2$ )  $\delta$  7.77 (s, 1H), 7.53 (s, 1H), 4.97 (s, 2H), 4.63 (s, 2H), 4.00 (s, 3H), 3.62 (dd,  $J=13.2$ , 6.7, 2H), 2.92 (t,  $J=6.7$ , 2H);  $^{13}\text{C-NMR}$  (100 MHz,  $\text{CO}(\text{CD}_3)_2$ )  $\delta$  168.5, 155.5, 146.5, 136.5, 126.1, 112.6, 111.1, 70.0, 68.1, 56.8, 38.9, 38.7.

**Synthesis of compound 5.** A mixture of alcohol **4** (0.24 g, 0.75 mmol), succinic anhydride (0.083 g, 0.83 mmol) and DMAP (0.1 g, 0.83 mmol) in THF (5 mL) was stirred for 24 h at room temperature. Water was added, and the pH adjusted with HCl (1M) to 2–3. The aqueous phase was extracted with EtOAc and the organic phase dried and evaporated to yield a solid **5** (0.22 g, 0.53 mmol, 70 % yield) (Scheme S1).  $^1\text{H-NMR}$  (400 MHz,  $\text{CO}(\text{CD}_3)_2$ )  $\delta$  7.79 (s, 1H), 7.24 (s, 1H), 5.49 (s, 2H), 4.66 (s, 2H), 4.02 (s, 3H), 3.62 (dd,  $J=12.7$ , 6.5, 2H), 2.92 (t,  $J=6.5$ , 2H), 2.75 (m, 2H), 2.68 (m, 2H);  $^{13}\text{C-NMR}$  (100 MHz,  $\text{CO}(\text{CD}_3)_2$ )  $\delta$  174.0, 172.7, 168.6, 155.4, 147.2, 140.4, 129.8, 112.6, 111.6, 69.7, 63.5, 57.1, 38.9, 38.8, 30.7, 30.6.

**Synthesis of gold nanostars (AuNSts).** Gold nanostars were synthesized by seeded growth method using PVP solution in DMF. At 25 °C, 50  $\mu\text{L}$  of an aqueous solution of 166 mM  $\text{HAuCl}_4$  was mixed with 15 mL of 20 mM PVP solution in DMF. After 5 min, 10  $\mu\text{L}$  of preformed seed dispersion (15 nm gold nanospheres coated with PVP in ethanol,  $[\text{Au}] = 6.5 \text{ mM}$ ) was added and allowed to react for 24 hours without stirring. Gold nanoparticles were recovered by centrifugation (20 min, 9500 rpm) and washed five times with water by centrifugation and redispersion. The concentration of Au in all gold colloids was derived from their extinction spectra (absorbance at 400 nm).

**Synthesis of mesoporous silica nanoparticles (MSNP).** 1.0 g (2.74 mmol) of CTAB was dissolved in 480 mL of deionized water. Then, the pH was increased by adding 3.5 mL of a 2 M NaOH solution and the temperature was increased to 80 °C. TEOS (5.0 mL, 22.4 mmol) was then added dropwise to this solution. Magnetic stirring was kept for 2 h to give a white precipitate. Finally, the solid was isolated by centrifugation, washed several times with water and dried at 60 °C overnight. To obtain the final mesoporous nanoparticles (**MSNP**), the as-synthesized solid was calcined at 550 °C using an oxidant atmosphere for 5 h in order to remove the surfactant.

**Synthesis of Janus N1 nanoparticles.** **MSNP** (180 mg) were dispersed in 9 mL of aqueous solution (6.7 % ethanol) and CTAB was added for a 1  $\mu\text{M}$  final concentration. The mixture was heated at 75 °C, and then 1 g of paraffin wax was added. Once the paraffin was melted, the mixture was vigorously stirred for 15 minutes using an Ultra-Turrax T-8 homogenizer (IKA). Afterward, the mixture was further stirred for 1 h at 1500 rpm and 75 °C using a magnetic stirrer. The resulting Pickering emulsion was then cooled to room temperature, diluted with 9 mL of methanol and reacted with 180  $\mu\text{L}$  of (3-mercaptopropyl)triethoxysilane for 3 h. The solid (**HS-MSNP**) was collected by centrifugation, washed with hexane and finally dried at 60 °C overnight. The partially mercapto-functionalized **MSNP** (**HS-MSNP**, 10 mg) were dispersed in 1.5 mL of acetonitrile, followed by the addition of 50  $\mu\text{L}$  of (3-iodopropyl)trimethoxysilane. The solution was stirred at 25 °C for 18 h. The iodopropyl-modified **MSNP** (**HS-MSNP-I**) were collected via centrifugation and washed with ACN. Then, the nanoparticles were re-suspended in 1.5 mL of anhydrous DMF,

in which 20 mg of benzimidazole and 20  $\mu\text{L}$  of triethylamine were added. The solution was stirred at 70 °C for 24 h. The nanoparticles (**HS-MSNP-Bzi**) were collected via centrifugation and washed with DMF and H<sub>2</sub>O. The nanoparticles were mixed with 1.5 mL of Dox in aqueous solution (2 mg mL<sup>-1</sup>). The suspension was stirred for 18 h before  $\beta$ -cyclodextrin (40 mg) was added. The mixture was stirred for another 18 h, and the nanoparticles (**HS-MCM@Dox@Bzi-CD**) were centrifuged and washed with H<sub>2</sub>O. For gold attachment, **AuNSts** were dispersed in 2 mL of compound **6** solution in THF and stirred for 18 h. **AuNSt@PLM-COOH** nanoparticles were collected by centrifugation, washed with THF and re-dispersed in H<sub>2</sub>O. **HS-MCM@Dox@Bzi-CD** nanoparticles were dispersed in 0.5 mL of H<sub>2</sub>O and added over 1.5 mL of the **AuNSt@PLM-COOH** suspension in H<sub>2</sub>O. The mixture was stirred overnight, collected by centrifugation, washed with H<sub>2</sub>O and dried.

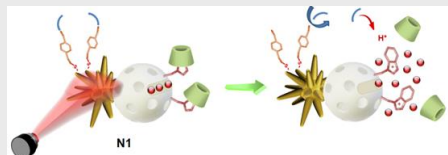
## Acknowledgements

The authors gratefully acknowledge financial support from the Spanish Government (Projects MAT2015-64139-C4-1-R, AGL2015-70235-C2-2-R and SAF2017-84689-R (MINECO/AEI/FEDER, UE)), the Generalitat Valenciana (Project PROMETEO2018/024) and European Union (Programme European Union- Action 2- Erasmus Mundus Partnerships, GRANT AGREEMENT NUMBER - 2014 - 0870 / 001 – 001). A. H. thanks Erasmus Mundus Programme for his PhD scholarship at EurolinkaNet project. A. L.-L. thanks “La Caixa” Banking Foundation for his PhD scholarship. The authors thank UPV electron microscopy and CIPF confocal and electron microscopy services for technical support.

**Keywords:** NIR light • drug delivery • light-responsive nanodevices • mesoporous silica • gold nanostars

- [1] P. Yang, S. Gai, J. Lin, *Chem. Soc. Rev.* **2012**, *41*, 3679-3698.
- [2] F. Sancenón, Ll. Pascual, M. Oroval, E. Aznar, R. Martínez-Máñez, *ChemOpen* **2015**, *4*, 418-437.
- [3] C. Giménez, E. Climent, E. Aznar, R. Martínez-Máñez, F. Sancenón, M. D. Marcos, P. Amorós, K. Rurack, *Angew. Chem. Int. Ed.* **2014**, *53*, 12629-12633.
- [4] A. Llopis-Lorente, P. Díez, A. Sánchez, M. D. Marcos, F. Sancenón, P. Martínez-Ruiz, R. Villalonga, R. Martínez-Máñez, *Nature Commun.* **2017**, *8*, 15511-15517.
- [5] N. Song, Y. -W. Yang, *Chem. Soc. Rev.* **2015**, *44*, 3474-3504.
- [6] E. Aznar, M. Oroval, Ll. Pascual, J. R. Murguía, R. Martínez-Máñez, F. Sancenón, *Chem. Rev.* **2016**, *116*, 561-718.
- [7] S. Koutsopoulos, *Adv. Drug Delivery Rev.* **2012**, *64*, 1459-1476.
- [8] G. Bao, S. Mitragotri, S. Tong, *Annu. Rev. Biomed. Eng.* **2013**, *15*, 253-282.
- [9] A. Hernández Monoto, R. Montes, A. Samadi, M. Gorbe, J. M. Terrés, R. Cao-Milám, E. Aznar, J. Ibañez, R. Masot, M. D. Marcos, M. Orzáez, F. Sancenón, L. Oddershede, R. Martínez-Máñez, *ACS Appl. Mater. Interfaces* **2018**, *10*, 27644-27656.
- [10] C. de la Torre, L. Domínguez-Berrocal, J. R. Murguía, M. D. Marcos, R. Martínez-Máñez, J. Bravo, F. Sancenón, *Chem. Eur. J.* **2018**, *24*, 1890-1897.
- [11] A. H. Teruel, E. Pérez-Esteve, I. González-Álvarez, M. González-Álvarez, A. M. Costero, D. Ferrí, M. Parra, P. Gavíña, V. Merino, R. Martínez-Máñez, F. Sancenón, *J. Control. Release* **2018**, *281*, 58-69.
- [12] A. García-Fernández, G. García-Laínez, M. L. Ferrández, E. Aznar, F. Sancenón, M. J. Alcaraz, J. R. Murguía, M. D. Marcos, R. Martínez-Máñez, A. M. Costero, M. Orzáez, *J. Control. Release* **2017**, *248*, 60-70.
- [13] S. K. Rastogi, H. E. Anderson, J. Lamas, S. Barret, T. Cantu, S. Zauscher, W. J. Brittain, T. Betancourt, *ACS Appl. Mater. Interfaces* **2018**, *10*, 30071-30080.
- [14] M. Martínez-Carmona, D. Lozano, A. Baeza, M. Colilla, M. Vallet-Regí, *Nanoscale* **2017**, *9*, 15967-1597.
- [15] U. Mahmood, R. Weissleder, *Mol. Cancer Ther.* **2003**, *2*, 489-496.
- [16] R. A. Weissleder, *Nature Biotechnol.* **2001**, *19*, 316-317.
- [17] M. R. Hamblin, T. N. Demidova, *Proc. SPIE* **2006**, *6140*, 614001-614013.
- [18] G. Jalani, R. Naccache, D. H. Rosenzweig, L. Haglund, F. Vetrone, M. Cerruti, *J. Am. Chem. Soc.* **2016**, *138*, 1078-1083.
- [19] B. Yan, J. -C. Boyer, N. R. Branda, Y. Zhao, *J. Am. Chem. Soc.* **2011**, *133*, 19714-19717.
- [20] N. Z. Knezevic, V. S. -Y. Lin, *Nanoscale* **2013**, *5*, 1544-1551.
- [21] S. Ibsen, E. Zahavy, W. Wrasdilo, M. Berns, M. Chan, S. Esener, *Pharm. Res.* **2010**, *27*, 1848-1860.
- [22] A. Patchornik, B. Amit, R. B. Woodward, *J. Am. Chem. Soc.* **1970**, *92*, 6333-6335.
- [23] B. Amit, U. Zehavi, A. Patchornik, *J. Org. Chem.* **1974**, *39*, 192-196.
- [24] X. Bai, Z. Li, S. Jockusch, N. J. Turro, J. Ju, *Proc. Natl. Acad. Sci. USA* **2003**, *100*, 409-413.
- [25] S. Laimgruber, W. J. Schreier, T. Schrader, F. Koller, W. Zinth, P. Gilch, *Angew. Chem. Int. Ed.* **2005**, *44*, 7901-7904.
- [26] N. Fomina, C. McFearin, M. Sermsakdi, O. Edigin, A. Almutairi, *J. Am. Chem. Soc.* **2010**, *132*, 9540-9542.
- [27] Q. Lin, Q. Huang, C. Li, C. Bao, Z. Liu, F. Li, L. Zhu, *J. Am. Chem. Soc.* **2010**, *132*, 10645-10647.
- [28] I. Aujard, C. Benbrahim, M. Gouget, O. Ruel, J. -B. Baudin, P. Neveu, L. Jullien, *Chem. Eur. J.* **2006**, *12*, 6865-6879.
- [29] J. Zhao, T. D. Gover, S. Muralidharan, D. A. Auston, D. Weinreich, J. P. Y. Kao, *Biochemistry* **2006**, *45*, 4915-4926.
- [30] I. Cohanachi, F. E. Hernández, *J. Phys. Chem. B* **2005**, *109*, 14506-14512.
- [31] V. Voliani, F. Ricci, G. Signore, R. Nifosi, S. Luin, F. Beltram, *Small* **2011**, *7*, 3271-3275.
- [32] V. Voliani, G. Signore, O. Vittorio, P. Faraci, S. Luin, J. Perez-Prieto, F. Beltram, *J. Mater. Chem. B* **2013**, *1*, 4225-4230.
- [33] A. Llopis-Lorente, B. de Luis, A. García-Fernández, P. Díez, A. Sánchez, M. D. Marcos, R. Villalonga, R. Martínez-Máñez, F. Sancenón, *J. Mater. Chem. B* **2017**, *5*, 6734-6739.
- [34] A. Llopis-Lorente, P. Díez, C. de la Torre, A. Sánchez, F. Sancenón, E. Aznar, M. D. Marcos, P. Martínez-Ruiz, R. Martínez-Máñez, R. Villalonga, *Chem. Eur. J.* **2017**, *23*, 4276-4281.
- [35] A. Llopis-Lorente, B. de Luis, A. García-Fernández, S. Jimenez-Falcao, M. Orzáez, F. Sancenón, R. Villalonga, R. Martínez-Máñez, *ACS Appl. Mater. Interfaces* **2018**, *10*, 26494-26500.
- [36] S. Trigari, A. Rindi, G. Margheri, S. Sottini, G. Dellepiane, E. Giorgetti, *J. Mater. Chem.* **2011**, *21*, 6531-6540.
- [37] P. S. Kumar, I. Pastoriza-Santos, B. Rodríguez-González, F. J. García de Abajo, L. M. Liz-Marzán, *Nanotechnology* **2008**, *19*, 015606-015612.
- [38] A. Guerrero-Martínez, S. Barbosa, I. Pastoriza-Santos, L. M. Liz-Marzán, *Curr. Opin. Colloid Interface Sci.* **2011**, *16*, 118-127.
- [39] F. Hao, C. L. Nehl, J. H. Hafner, P. Nordlander, *Nano Lett.* **2007**, *7*, 729-732.
- [40] E. Aznar, R. Villalonga, C. Giménez, F. Sancenón, M. D. Marcos, R. Martínez-Máñez, P. Díez, J. M. Pingarrón, P. Amorós, *Chem. Commun.* **2013**, *49*, 6391-6393.
- [41] E. Aznar, M. D. Marcos, R. Martínez-Máñez, F. Sancenón, J. Soto, P. Amorós, C. Gullem, *J. Am. Chem. Soc.* **2009**, *131*, 6833-6843.
- [42] P. Klán, T. Šolomek, C. G. Bochet, A. Blanc, R. Givens, M. Rubina, V. Popik, A. Kostikov, J. Wirz, *Chem. Rev.* **2013**, *113*, 119-191.
- [43] S. Rittikulitthai, C. Soon Park, M. D. Marquez, A. C. Jamison, T. Frank, C.-H. Wu, J. I. Wu, T. R. Lee, *Langmuir* **2018**, *34*, 6645-6652.

## COMMUNICATION



NIR irradiation of AuNSTs-MSNs nanodevice induced succinic acid generation and doxorubicin release due to a dethreading of a supramolecular nanovalve

A. Hernández Montoto, A. Llopis-Lorente, M. Gorbe, J. M. Terrés, R. Cao-Milán, B. Díaz de Greñu, M. Alfonso, J. Ibañez, M. D. Marcos, M. Orzáez, R. Villalonga, R. Martínez-Máñez\* and F. Sancenón

Page No. – Page No.

Janus gold nanostars-mesoporous silica nanoparticles for NIR light-triggered drug delivery